



ARTICLE

Alflutinin (AST2818), primarily metabolized by CYP3A4, is a potent CYP3A4 inducer

Xiao-yun Liu^{1,2}, Zi-tao Guo¹, Zhen-dong Chen^{1,2}, Yi-fan Zhang¹, Jia-lan Zhou¹, Yong Jiang³, Qian-yu Zhao³, Xing-xing Diao^{1,2} and Da-fang Zhong^{1,2}

Alflutinin (AST2818) is a third-generation epidermal growth factor receptor (EGFR) inhibitor that inhibits both EGFR-sensitive mutations and T790M mutations. Previous study has shown that after multiple dosages, alflutinin exhibits nonlinear pharmacokinetics and displays a time- and dose-dependent increase in the apparent clearance, probably due to its self-induction of cytochrome P450 (CYP) enzyme. In this study, we investigated the CYP isozymes involved in the metabolism of alflutinin and evaluated the enzyme inhibition and induction potential of alflutinin and its metabolites. The data showed that alflutinin in human liver microsomes (HLMs) was metabolized mainly by CYP3A4, which could catalyze the formation of AST5902. Alflutinin did not inhibit CYP isozymes in HLMs but could induce CYP3A4 in human hepatocytes. Rifampin is a known strong CYP3A4 inducer and is recommended by the FDA as a positive control in the CYP3A4 induction assay. We found that the induction potential of alflutinin was comparable to that of rifampin. The E_{max} of CYP3A4 induction by alflutinin in three lots of human hepatocytes were 9.24-, 11.2-, and 10.4-fold, while the fold-induction of rifampin (10 μ M) were 7.22-, 19.4- and 9.46-fold, respectively. The EC_{50} of alflutinin-induced CYP3A4 mRNA expression was 0.25 μ M, which was similar to that of rifampin. In addition, AST5902 exhibited much weak CYP3A4 induction potential compared to alflutinin. Given the plasma exposure of alflutinin and AST5902, both are likely to affect the pharmacokinetics of CYP3A4 substrates. Considering that alflutinin is a CYP3A4 substrate and a potent CYP3A4 inducer, drug–drug interactions are expected during alflutinin treatment.

Keywords: alflutinin; AST5902; CYP3A4; metabolism; enzyme induction; drug–drug interaction

Acta Pharmacologica Sinica (2020) 41:1366–1376; <https://doi.org/10.1038/s41401-020-0389-3>

INTRODUCTION

Lung cancer is the most commonly diagnosed cancer (11.6% of the total cases of cancer) and the leading cause of cancer death globally (18.4% of the overall cancer-related deaths) [1]. In China, the most common cause of cancer-related deaths is lung cancer (24.1%) [2]. Approximately 80%–85% of lung cancer types are non-small cell lung cancer (NSCLC), and the most common subtypes of NSCLC are lung adenocarcinoma (LUAD) and lung squamous cell carcinoma (LUSC) [3–5]. Epidermal growth factor receptor (EGFR) and Kirsten-RAS (*KRAS*) gene mutations are more common in LUAD, while in LUSC, the more common mutations are cyclin-dependent kinase inhibitor 2A (*CDKN2A*) and tumor suppressor protein p53 (*TP53*) [6]. EGFR is also known as HER or ErbB1, which contains HER2 (ErbB2), HER3 (ErbB3) and HER4 (ErbB4) in its family [7]. The clustering of mutations in the ATP-binding pocket of EGFR may lead to its constitutive, ligand-independent activation [8]. The gain-of-sensitivity mutations include exon 19 deletion (amino acid residues 747–750) and the L858R mutation (nucleotide substitutions on exon 21) [9]. Hence, targeted therapy for the management of NSCLC with EGFR mutations is of epoch-making significance.

First-generation EGFR tyrosine kinase inhibitors (TKIs), namely, erlotinib and gefitinib, exert better clinical effects than

conventional cytotoxic therapy [10, 11]. Second-generation pan-HER EGFR TKIs, such as afatinib and dacomitinib, are notably different from first-generation EGFR TKIs, which reversibly compete with ATP. Afatinib and dacomitinib can improve the median progression-free survival (PFS) of NSCLC with sensitive EGFR mutations compared to gefitinib and erlotinib [12–15]. Secondary or acquired resistance to first-generation EGFR TKIs has been extensively studied. For instance, a threonine-to-methionine substitution at position 790 (T790M) in exon 20 can increase ATP affinity in the ATP pocket [16]. Third-generation EGFR TKIs covalently bind to cysteine 797 and target both sensitizing and T790M-specific mutations while sparing wild-type EGFR [17, 18]. Osimertinib, a third-generation EGFR inhibitor, not only exhibits efficacy that is superior to platinum-based therapy plus pemetrexed in NSCLC patients harboring the T790M mutation but also displays greater efficacy in EGFR mutation-positive advanced NSCLC patients compared to standard EGFR TKIs [19, 20]. In addition, olmutinib has been launched in South Korea for the treatment of patients with locally advanced or metastatic EGFR T790M mutation-positive NSCLC [21].

Alflutinin, also known as AST2818, is a third-generation EGFR inhibitor. A phase III clinical trial (FLAG, NCT03787992) is being conducted in China to assess whether alflutinin can serve as the

¹State Key Laboratory of Drug Research, Shanghai Institute of Materia Medica, Chinese Academy of Sciences, Shanghai 201210, China; ²University of Chinese Academy of Sciences, Beijing 100049, China and ³Shanghai Allist Pharmaceuticals Inc., Shanghai 201203, China
Correspondence: Xing-xing Diao (xxdiao@simm.ac.cn) or Da-fang Zhong (dfzhong@simm.ac.cn)

Received: 2 November 2019 Revised: 19 February 2020 Accepted: 20 February 2020

Published online: 31 March 2020

first-line treatment for locally advanced or metastatic NSCLC patients compared with gefitinib. Data from phase I/II clinical trials have demonstrated that alflutinin is generally well tolerated and exhibits significant clinical efficacy in NSCLC patients with the T790M mutation who progressed after EGFR-TKI therapy [22]. The *N*-desmethyl metabolite AST5902 has been identified as the principal metabolite of alflutinin both in vitro and in vivo, which exerts remarkable antineoplastic activity similar to alflutinin (from a PK report in the phase I clinical study). Although alflutinin displays linear pharmacokinetics within the doses of 20–240 mg after single dose administration, its nonlinear pharmacokinetics and the accumulation of AST5902 have been observed after multiple dosing [23]. Alflutinin displays a time- and dose-dependent increase in clearance (CL/F) following multiple doses, probably due to its self-induction through a cytochrome P450 (CYP) enzyme. Thus, the assessment of CYP enzymes involved in alflutinin biotransformation and the evaluation of CYP enzyme induction can help to understand the metabolism of alflutinin in vivo and further estimate potential drug–drug interactions (DDIs).

This study aimed to (i) elucidate the in vitro metabolism of alflutinin and its metabolites, (ii) identify the major metabolic enzymes involved in their metabolism, and (iii) evaluate the enzyme inhibition and induction potential of alflutinin and its metabolites. The findings would generate more reliable biotransformation information on alflutinin and provide evidence to support clinical DDI decision making.

MATERIALS AND METHODS

Materials

Alflutinin was provided by Shanghai Allist Pharmaceuticals Inc. (Shanghai, China). The following chemicals were purchased from Meilun Biotechnology Co., Ltd. (Dalian, China): 1-aminobenzotriazole (ABT), 6 α -hydroxy paclitaxel, α -naphthoflavone, acetaminophen-*d*₄, chlormethiazole, ketoconazole, quercetin, quinidine, sulfaphenazole and ticlopidine. 5-Mephenytoin and 6 β -hydroxytestosterone were supplied by BD Gentest Corporation (Woburn, MA, USA). Phenacetin, tolbutamide, dextromethorphan, *O*-desmethyl dextromethorphan, 4'-hydroxymefentoin, paclitaxel and 1'-hydroxymidazolam were purchased from Sigma Chemical Co. Ltd. (St. Louis, MO, USA). Bupropion and hydroxy bupropion were supplied by Toronto Research Chemicals Inc. (Toronto, Canada). Testosterone was obtained from Sigma-Aldrich (St. Louis, MO, USA). 4'-Hydroxytolbutamide was provided by the Department of Microbiology, Shenyang Pharmaceutical University (Shenyang, China). Nicotinamide adenine dinucleotide phosphate (NADPH; reduced form) and midazolam were obtained from Roche Inc. (Mannheim, Germany). HPLC-grade ammonium acetate and formic acid were supplied by Roe Scientific Inc. (Neward, NJ, USA) and Tokyo Chemical Industry Co., Ltd. (Tokyo, Japan), respectively, while HPLC-grade acetonitrile and methanol were supplied by Merck KGaA (Darmstadt, Germany). Dimethyl sulfoxide (DMSO) was supplied by Sinopharm Chemical Reagent Co., Ltd. (Shanghai, China). A Milli-Q system was used to prepare deionized H₂O (Molsheim, France). Recombinant human cytochrome P450 (CYP) isozymes (e.g., 1A2, 2A6, 2B6, 2C8, 2C9, 2C19, 2D6, 2E1, 3A4, and 3A5) as well as pooled human liver microsomes (HLMs) were purchased from Corning Inc. (New York, NY, USA). Primary hepatocytes (lot #DJJ, Caucasian male; 51 years of age; lot #QBU, Caucasian male; 50 years of age; and lot #HVN, Caucasian male; 33 years of age) were purchased from BioIVT (Baltimore, MD, USA).

Metabolism of alflutinin in HLMs

Before starting the experiments, the HLMs were thawed gently on ice. Then, 3 μ M alflutinin was added to the HLMs (0.5 mg protein/mL) in 100 mM phosphate-buffered saline (PBS; pH 7.4) to a total volume

of 100 μ L. After incubating at 37 °C for 3 min, the reactions were initiated by the addition of 1.0 mM NADPH. Following 1 h of incubation, the reactions were terminated by mixing with ice-cold acetonitrile at the same volume. All incubations were performed in duplicate and then analyzed by UPLC-UV/Q-TOF MS.

Incubation of HLMs with specific CYP inhibitors

HLMs were used to study the effects of CYP enzyme inhibitors on the metabolism of alflutinin. The incubation mixture (100 μ L) consisted of alflutinin (3 μ M), HLMs (0.5 mg protein/mL), NADPH (1 mM), PBS (100 mM, pH 7.4) and a selective CYP inhibitor. The chemical inhibitors were as follows: α -naphthoflavone (2 μ M) for CYP1A/2C, quercetin (20 μ M) for CYP2C8, sulfaphenazole (6 μ M) for CYP2C9, ticlopidine (24 μ M) for CYP2B6/2C19, quinidine (8 μ M) for CYP2D6, chlormethiazole (24 μ M) for CYP2E1, ketoconazole (2 μ M) for CYP3A and ABT (1 mM) for all CYP enzymes. These inhibitors were preincubated with HLMs in the presence of NADPH for 10 min before adding the substrate. After that, the reactions were initiated by incubation at 37 °C for 60 min. Finally, the reactions were terminated by the addition of 100 μ L of ice-cold acetonitrile. All incubations were performed in duplicate, and the formation of metabolites was evaluated in the absence or presence of inhibitors.

The metabolism of alflutinin through recombinant human CYP isoenzyme

To identify the specific isoform that participates in the metabolism of alflutinin, 3 μ M alflutinin was mixed with recombinant human CYP1A2, 2A6, 2B6, 2C8, 2C9, 2C19, 2D6, 2E1, 3A4, or 3A5 (25 pmol P450/mL) in a total volume of 100 μ L. The reactions were initiated and terminated by the addition of 1 mM NADPH and 100 μ L of ice-cold acetonitrile, respectively. The incubation was carried at 37 °C for 60 min. All reactions were conducted in duplicate, followed by UPLC-UV/Q-TOF MS analysis.

UPLC-UV/Q-TOF MS detection

The different metabolites of alflutinin were detected with an ACQUITY UPLC HSS T3 column (1.8 μ m, 100 mm \times 2.1 mm, Waters Corp., Milford, MA, USA) using a Waters ACQUITY UPLC system (Milford, MA, USA). The mobile phase contained a mixture of 5 mM ammonium acetate with 0.05% formic acid (A) and acetonitrile (B). The gradient elution program was as follows: 5% B (1 min), 60% B (10 min), 95% B (1 min and hold for 1 min) and a 5% B (1 min and hold for 2 min) for column re-equilibration. The flow rate was set to 0.4 mL/min, and the column temperature was maintained at 40 °C. Eluted fractions were monitored by a UV detector at 280 nm.

MS detection was carried out using a Waters SYNAPT G2 Q-TOF mass spectrometer (Milford, MA, USA) in positive ion electrospray ionization (ESI) mode. The desolvation gas flow and temperature were set to 800 L/h and 450 °C, respectively. The cone gas flow was adjusted to 50 L/h, and the source temperature was maintained at 120 °C. The capillary voltage and cone voltage were maintained at 3.0 kV and 40 V, respectively. The SYNAPT G2 MS system was operated under resolution mode (>20,000 at full width half maximum). The rate of data acquisition was 0.3 s/scan, and all data were collected within 13 min under MS^E acquisition mode. In the low-energy scan, the transfer CE and trap CE were 4 V and 6 V, respectively. In the high-energy scan, the transfer CE was 20 V, and the trap CE ramped from 20 to 25 V. The MS was calibrated at 1 ppm and operated through the leucine enkephalin Lockspray. MS data were acquired under continuum mode within a *m/z* range of 50–1200. MassLynx version 4.1 and UNIFI Portal software (Waters Corp., Milford, MA, USA) were employed for data processing.

Enzyme inhibition of alflutinin on major human CYP enzymes

All CYP isoform-specific probes, such as phenacetin, bupropion, paclitaxel, tolbutamide, 5-mephenytoin and dextromethorphan

(for CYP1A2, 2B6, 2C8, 2C9, 2C19, and 2D6, respectively), as well as midazolam and testosterone (for CYP3A4), were dissolved in methanol. Alflutinin was dissolved in DMSO as a 100 mM stock solution. The total volume was 100 μ L, and the medium was 100 mM PBS containing mixed HLMs (0.5 mg/mL), probe substrates, NADPH (1 mM) and different concentrations of alflutinin (0, 0.1, 0.33, 1, 3.30, 10, 33.3, and 100 μ M). The reactions were preincubated at 37 °C for 5 min. Under the experimental conditions, the enzyme concentration and incubation time of the reaction system were all within a linear range (Supplementary Table S1).

Enzyme induction of alflutinin and AST5902 on the human CYP3A4 enzyme

For the assessment of enzyme induction, 7×10^5 hepatocytes/mL were seeded into a collagen-coated 24-well plate and placed in a 37 °C humidified incubator with 5% CO₂ for 24 h. The hepatocytes were treated with the human CYP3A4 enzyme inducer rifampin (10 μ M), alflutinin or AST5902 (0.003, 0.01, 0.03, 0.1, 0.3, 1, 3 or 5 μ M) or 0.1% DMSO (control group) once daily for three consecutive days. After treatment, RNA extraction was performed with TRIzol (Invitrogen Life Technologies, Carlsbad, CA, USA) according to the manufacturer's protocol. cDNA synthesis was carried out using the PrimeScript RT reagent kit (Takara Bio Inc., Kusatsu, Japan). Real-time PCR was conducted on a StepOnePlus real-time PCR system (Applied Biosystems, Foster, CA, USA) using the SYBR green Premix Ex Taq kit (Takara Bio Inc., Kusatsu, Japan). The forward primer and reverse primer for CYP3A4 were 5'-ATCACTAGCACATCATTTGGAG-3' and 5'-GGAATGGAAAGTTATTGAGAG-3', respectively. For GAPDH, the forward and reverse primers were 5'-AGAAGGCTGGGGCTCATTTG-3' and 5'-GAGGGGC-CATCCACAGTCTTC-3', respectively. The levels of cDNA were quantitated by the comparative threshold cycle method using GAPDH as an internal standard. EC₅₀ is the concentration of inducer at 50% maximal effect of induction, which is obtained by a nonlinear regression test carried by GraphPad Prism version 5.0 (GraphPad Software Inc., San Diego, CA, USA).

RESULTS

UPLC/Q-TOF MS determination of alflutinin, AST5902 and AST28365

The chromatographic behaviors and MS fragmentation patterns of alflutinin and its metabolites AST5902 and AST28365 were first assessed to identify other potential alflutinin metabolites. Under the present chromatographic conditions, the retention time of alflutinin was found to be 9.37 min. In ESI(+) mode, alflutinin generated a protonated molecular ion [M + H]⁺ at m/z 569.261. Under higher-energy collision conditions, several fragment ions were observed at m/z 524.201 (–C₂H₇N), 441.192 (–C₂HF₃–C₂H₈N), 386.173 (–C₂HF₃–C₂H₉N–C₃H₂O), 370.172 (–C₂HOF₃–C₂H₉N–C₃H₂O), 302.102 (–C₂HF₃–C₅H₁₄N₂–C₃H₄ON–CH), 225.113 (C₁₃H₁₃N₄⁺) and 72.077 (C₄H₁₀N⁺, 100% abundance) for alflutinin (Fig. 1a). Based on the high-resolution mass spectral data, different tentative fragmentation patterns are illustrated in Fig. 1b. It was noted that the fragments of alflutinin were produced mainly by cleavage on the amine side chain, acrylamide and trifluoroethoxy moieties. In ESI (+) mode, AST5902 eluted at 9.09 min and generated a protonated molecule [M + H]⁺ at m/z 555.244. Under higher-energy collision conditions, several fragment ions were observed at m/z 498.186 (–C₃H₇N, 100% abundance), 415.179 (–C₂HF₃–C₃H₈N), 386.173 (–C₂HF₃–CH₇N–C₃H₂O), 360.154 (–C₂HF₃–C₃H₉N–C₃H₂O), 344.164 (–C₂HOF₃–C₃H₉N–C₃H₂O), 302.102 (–C₂HF₃–C₄H₁₂N₂–C₃H₄ON–CH) and 225.110 (C₁₃H₁₃N₄⁺) for AST5902 (Fig. 2a). Compared to alflutinin, the fragmentation ion at m/z 72.077 was absent, and the tentative fragmentation profile is illustrated in Fig. 2b. It was noted that the fragments of AST5902 were produced mainly by cleavage on the amine side chain, acrylamide and

trifluoroethoxy moieties. In addition, AST28365 eluted at 8.34 min and displayed a protonated molecular ion [M + H]⁺ at m/z 555.242. Under higher-energy collision conditions, several fragment ions were observed at m/z 510.181 (–C₂H₇N), 427.177 (–C₂HF₃–C₂H₈N), 372.156 (–C₂H₉N–C₂HF₃–C₃H₂O), 356.162 (–C₂H₉N–C₂HOF₃–C₃H₂O), 341.147 (–C₂H₉N–C₂HOF₃–C₃H₃ON), 288.089 (–C₂HF₃–C₅H₁₄N₂–C₃H₄ON–CH), 211.094 (C₁₂H₁₁N₄⁺) and 72.078 (C₄H₁₀N⁺, 100% abundance) for AST28365 (Fig. 3a). The different tentative fragmentation patterns are illustrated in Fig. 3b. It was noted that the fragments of AST28365 were produced mainly by cleavage on the amine side chain, acrylamide and trifluoroethoxy moieties.

Metabolism of alflutinin in HLMs

In the presence of NADPH, 13 metabolites were identified from the HLMs treated with alflutinin (Fig. 4). Compared with the inactive HLMs, the predominant metabolite was AST5902, which showed a retention time of 9.09 min. However, AST28365, which we predicted to be a major metabolite, was not detected in HLMs.

The data of the 13 detected metabolites, including the retention time, formula, observed and calculated m/z , MS area and fragment ions, are summarized in Table 1, and the structures of the 13 metabolites are illustrated in Fig. 5. The names of these metabolites were assigned according to their molecular weight, and the metabolites with similar molecular masses were sequentially named based on the order of retention time. The identities of the metabolites are displayed in the Supplementary Material.

The metabolism of alflutinin in recombinant human CYP isoenzymes

Alflutinin was hardly metabolized by some recombinant human CYP isoenzymes (e.g., 1A2, 2A6, 2B6, 2C8, 2C9, 2C19, 2D6, and 2E1), and only a few metabolites were produced during the metabolic process (Table 2). In contrast, alflutinin was extensively metabolized by CYP3A4. Specifically, the majority of phase I metabolites observed in HLMs were detected after 1-h exposure to CYP3A4, and at least 78% of alflutinin was transformed. Additionally, CYP3A5 was found to play a crucial role in the metabolism of alflutinin. Considering that CYP3A5 is less abundant than CYP3A4 in the liver, CYP3A4 has been regarded as the predominant enzyme involved in alflutinin metabolism. Similarly, the formation of AST5902 was catalyzed primarily by CYP3A4 but to a much lesser extent by CYP3A5. In addition, CYP2C8, CYP2C9, CYP2C19 and CYP2E1 could catalyze the formation of AST5902, although to a smaller extent. The relative contribution of the CYP450 subtypes to the metabolism of alflutinin and the formation of AST5902 was determined after normalization according to the relative amount of each CYP450 in human liver [24]. Based on the substrate (alflutinin) depletion method, alflutinin was found to be predominantly metabolized by CYP3A4 (78%), and with regard to the metabolite (AST5902) formation method, the principal enzyme contributing to AST5902 formation was identified as CYP3A4 (79%) (Supplementary Table S2).

Effects of CYP inhibitors on the formation of alflutinin metabolites in HLMs

The inhibitory effects of selective CYP inhibitors on the formation of alflutinin metabolites in HLMs were determined (Table 3). α -Naphthoflavone (CYP1A2 inhibitor) and chlormethiazole (CYP2E1 inhibitor) exhibited no significant effects on the formation of alflutinin metabolites. Quercetin (CYP2C8 inhibitor) suppressed the production of AST5902 by 68% and inhibited the formation of M486, M497 and M584-1 to a certain degree. Sulfaphenazole (CYP2C9 inhibitor) suppressed the production of AST5902 by 45% and exhibited little effect on the formation of other metabolites. Ticlopidine (inhibitor of CYP2B6 and CYP2C19) suppressed the production of AST5902 by 38% and inhibited the formation of M539, M554-1 and M555 to some extent. Quinidine (CYP2D6

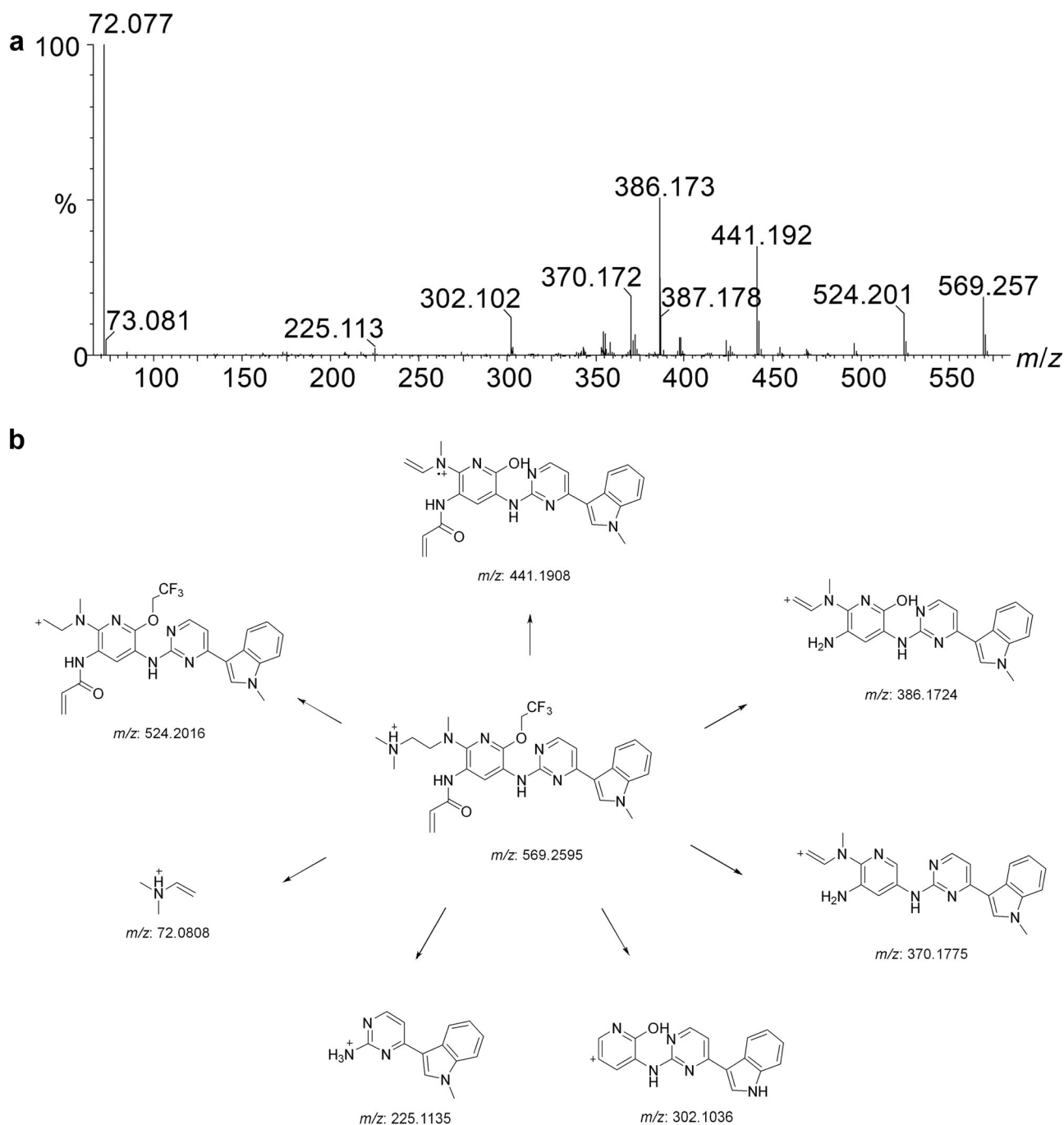


Fig. 1 The MS fragmentation patterns of alflutinib. Mass spectra of alflutinib under high-collision energy in positive detection mode (a), and their tentative fragmentation profiles (b)

inhibitor) suppressed the production of AST5902 by 46% and inhibited the formation of M484 and M497 to some extent. Ketoconazole (CYP3A4/5 inhibitor) and ABT (inhibitor of all CYP isoenzymes) suppressed the production of AST5902 by 86% and 98%, respectively. Except for M554-1, ketoconazole and ABT greatly suppressed the production of all the metabolites.

Altogether, the results of both CYP phenotyping assessments indicate that alflutinib is largely metabolized by the CYP3A4 enzyme.

Enzyme inhibition of alflutinib on major human CYP enzymes
The residual activities of the 7 CYP isozymes (i.e., CYP1A2, 2B6, 2C8, 2C9, 2C19, 2D6, and 3A4) in HLMs were all > 50% at the

maximum alflutinib concentration (100 μ M) in duplicate experiments (Table 4). Although IC_{50} values could not be determined, it was obvious that the values were more than 100 μ M.

Enzyme induction of alflutinib on the human CYP3A4 enzyme
The potential of alflutinib to induce CYP3A4 was assessed using primary human hepatocytes isolated from three lots (DJJ, QBU and HVN), and the results are presented in Table 5. It was noted that the maximum responses (net maximum fold increase, E_{max}) of alflutinib were 9.24-, 11.2- and 10.4-fold in DJJ, QBU and HVN, respectively. When DJJ, QBU and HVN were treated with 10 μ M rifampin for 72 h, the fold changes were 7.22-, 19.4-, and 9.46-fold, respectively. For DJJ and HVN, the mRNA expression level of

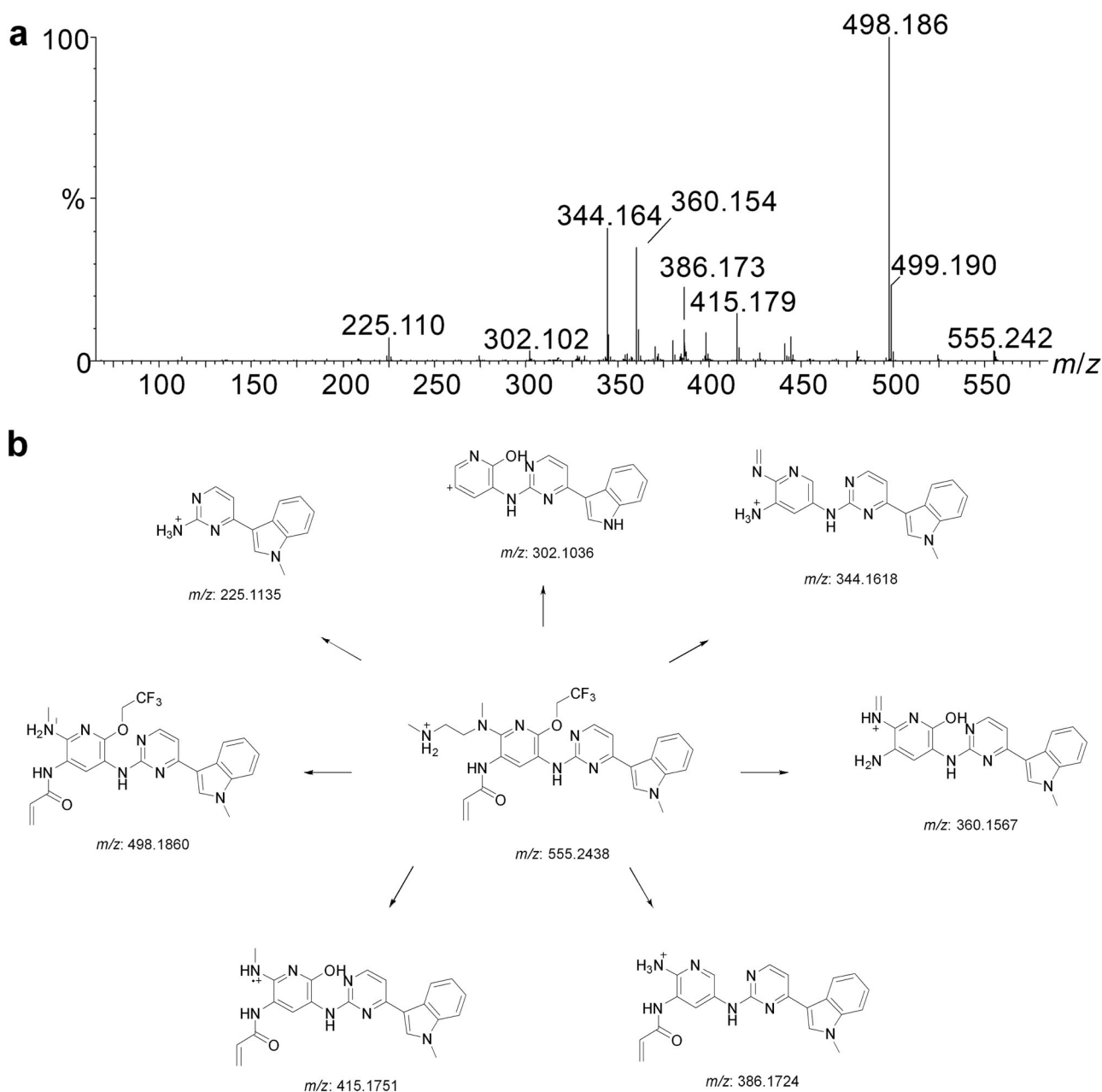


Fig. 2 The MS fragmentation patterns of AST5902. Mass spectra of AST5902 under high-collision energy in positive detection mode (**a**), and their tentative fragmentation profiles (**b**)

CYP3A4 increased with increasing alflutinib concentration in the range of 0.003–1 μM , while the mRNA expression level of CYP3A4 decreased when the alflutinib concentration was higher than 1 μM (Supplementary Fig. S11). For QBU, the mRNA expression level of CYP3A4 increased with increasing alflutinib concentrations in the range of 0.003–5 μM (Supplementary Fig. S11). As suggested by Fahmi and Ripp [25], when cell viability limits the acquisition of a full dose–response curve, the E_{max} can be regarded as the highest fold induction observed at a nontoxic concentration. To obtain the EC_{50} , a nonlinear regression test was carried out by GraphPad Prism version 5.0 (GraphPad Software Inc., San Diego, CA, USA). X represents the log of dose, Y indicates the fold change, and least squares fit was used as the fitting method. After treating DJJ and HVN with alflutinib at 3 and 5 μM for 72 h, a significant cell morphological change was observed under the microscope, and

cell survival decreased compared to the vehicle group. The dose–response curves of DJJ and HVN were bell-shaped, which could result from cytotoxicity or other factors [25]. Thus, the highest two concentrations were excluded from the nonlinear regression analysis [25]. However, the dose–response curve from HVN did not exhibit a sigmoidal curve, which overruled the EC_{50} value (Fig. 6). Therefore, the EC_{50} is presented as the concentration at 50% of the E_{max} .

According to the FDA guidelines (<https://www.fda.gov/media/108130/download>), we calculated the value of R_3 (the AUC ratio of a victim drug with or without CYP inducer) using Eq. 1, where the value of d is assumed to be 1 and the E_{max} is the maximal in vitro inductive effect. The C_{max} of alflutinib (80 mg) was 108 nM at steady state [22]. Given the low recovery of alflutinib in plasma at 37 $^{\circ}\text{C}$ after 6 h, plasma protein binding could not be determined

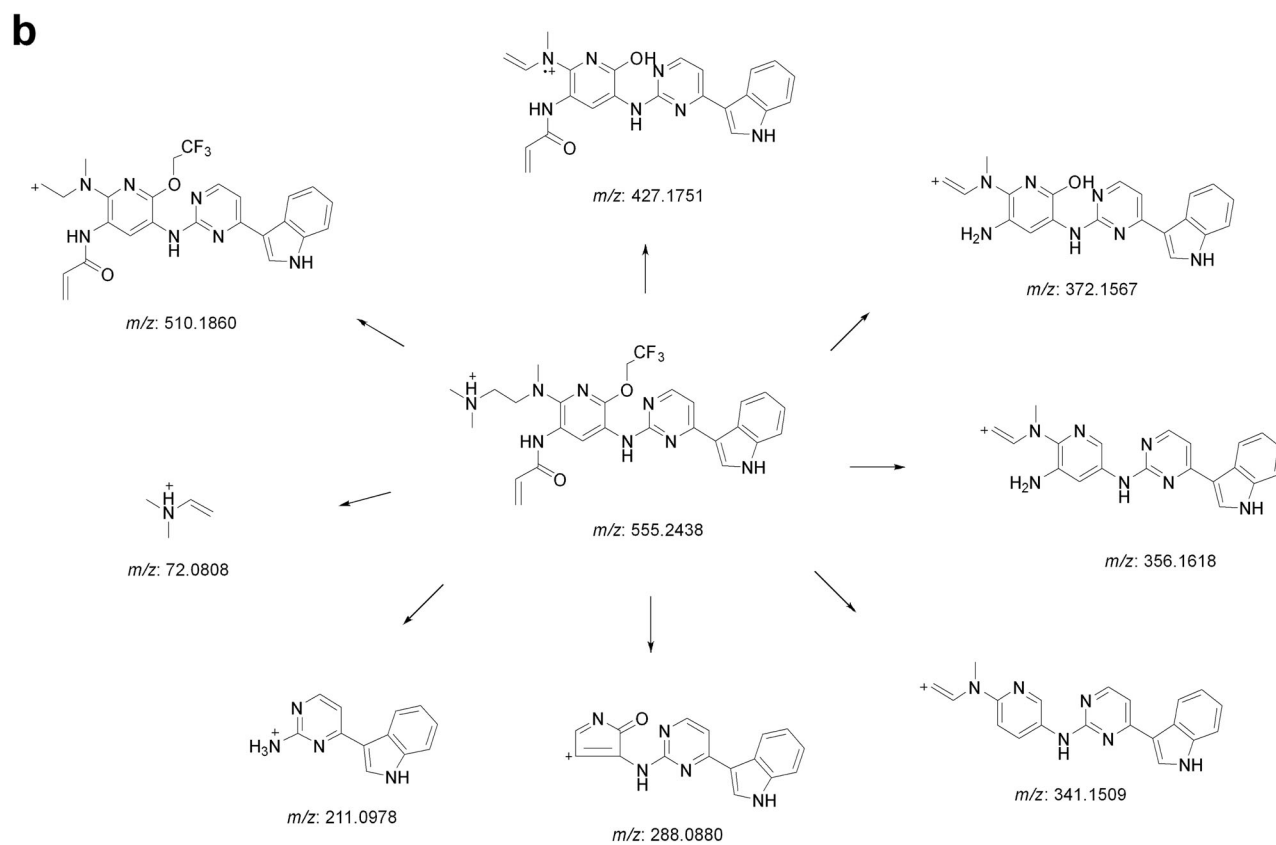
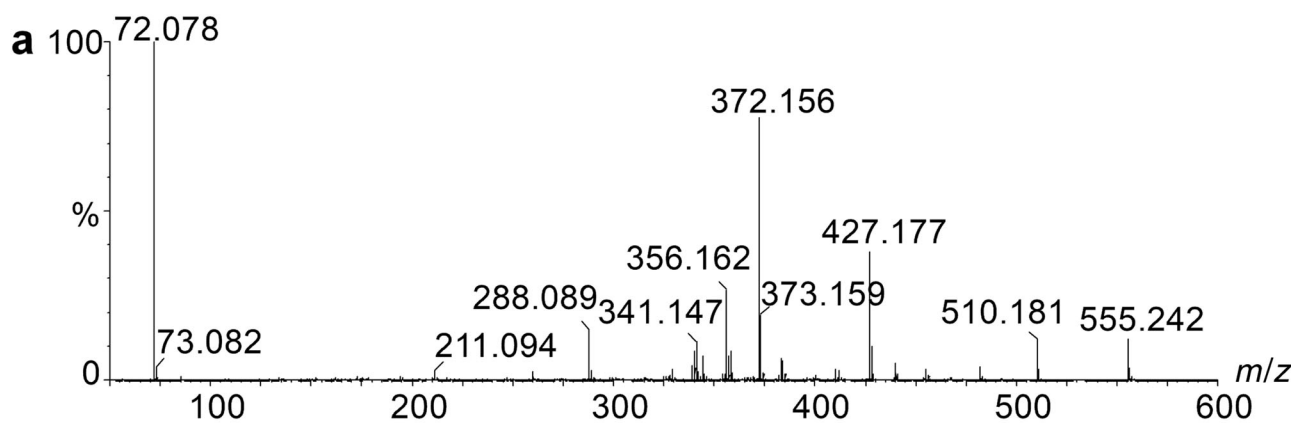


Fig. 3 The MS fragmentation patterns of AST28365. Mass spectra of AST28365 under high-collision energy in positive detection mode (a), and their tentative fragmentation profiles (b)

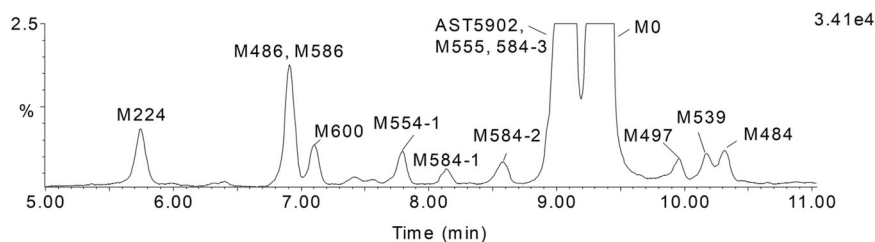


Fig. 4 Metabolic profiles of alflutinib in HLMs. The MS height of alflutinib was set as 100%, and the MS height of AST5902 is approximate 50% of alflutinib. The relative MS height of other metabolite to alflutinib was shown

Table 1. Characterization of alflutinib metabolites in HLMs through UPLC/Q-TOF MS

Name	Metabolic pathway	Retention time (min)	Formula	Observed (m/z)	Calculated (m/z)	Mass error (ppm)	MS area	Fragment ions
M224	N-Dealkylation	5.74	C ₁₃ H ₁₂ N ₄	225.1136	225.1135	0.6	2.32 × 10 ³	208.082
M486	O-Dealkylation	6.90	C ₂₆ H ₃₀ N ₈ O ₂	487.2567	487.2564	0.6	5.77 × 10 ³	442.198, 387.183, 372.162, 72.082
M586	Dioxidation of AST5902	6.92	C ₂₇ H ₂₉ F ₃ N ₈ O ₄	587.2332	587.2337	-0.7	9.00 × 10 ²	530.172, 512.165, 413.160, 358.140,
M600	Dioxidation	7.11	C ₂₈ H ₃₁ F ₃ N ₈ O ₄	601.249	601.2493	-0.5	2.60 × 10 ³	556.199, 473.184, 418.165, 72.081
M554-1	N-Demethylation	7.78	C ₂₇ H ₂₉ F ₃ N ₈ O ₂	555.244	555.2438	0.3	2.12 × 10 ³	510.181, 427.168, 372.156, 356.162, 225.109, 72.078
M584-1	Oxidation	8.14	C ₂₈ H ₃₁ F ₃ N ₈ O ₃	585.254	585.2544	-0.6	1.04 × 10 ³	541.208, 386.173, 370.172, 72.081
M584-2	Oxidation	8.59	C ₂₈ H ₃₁ F ₃ N ₈ O ₃	585.2544	585.2544	0	1.83 × 10 ³	457.188, 386.173, 72.081
M555	Oxidation and acetylation of M498	8.94	C ₂₆ H ₂₄ F ₃ N ₇ O ₄	556.1913	556.1915	-0.3	2.24 × 10 ³	498.186, 225.110
AST5902	N-Demethylation	9.09	C ₂₇ H ₂₉ F ₃ N ₈ O ₂	555.2442	555.2438	0.7	7.84 × 10 ⁴	498.186, 415.179, 386.173, 360.154, 344.164, 302.102, 225.110
M584-3	Oxidation	9.19	C ₂₈ H ₃₁ F ₃ N ₈ O ₃	585.2544	585.2544	0	1.74 × 10 ³	524.201, 441.183
M0	Parent	9.36	C ₂₈ H ₃₁ F ₃ N ₈ O ₂	569.2604	569.2595	1.6	2.47 × 10 ⁵	524.201, 441.192, 386.173, 370.172, 302.102, 225.113, 72.077
M497	N-Dealkylation	9.94	C ₂₄ H ₂₂ F ₃ N ₇ O ₂	498.1855	498.186	-1	1.49 × 10 ³	415.176, 360.159, 344.160, 302.098, 225.113
M539	Acetylation of M497	10.16	C ₂₆ H ₂₄ F ₃ N ₇ O ₃	540.1957	540.1965	-1.6	1.82 × 10 ³	398.169, 225.113
M484	Dealkylation and oxidation	10.3	C ₂₃ H ₁₉ F ₃ N ₆ O ₃	485.1548	485.1543	0.9	2.42 × 10 ³	467.142, 347.123, 225.113

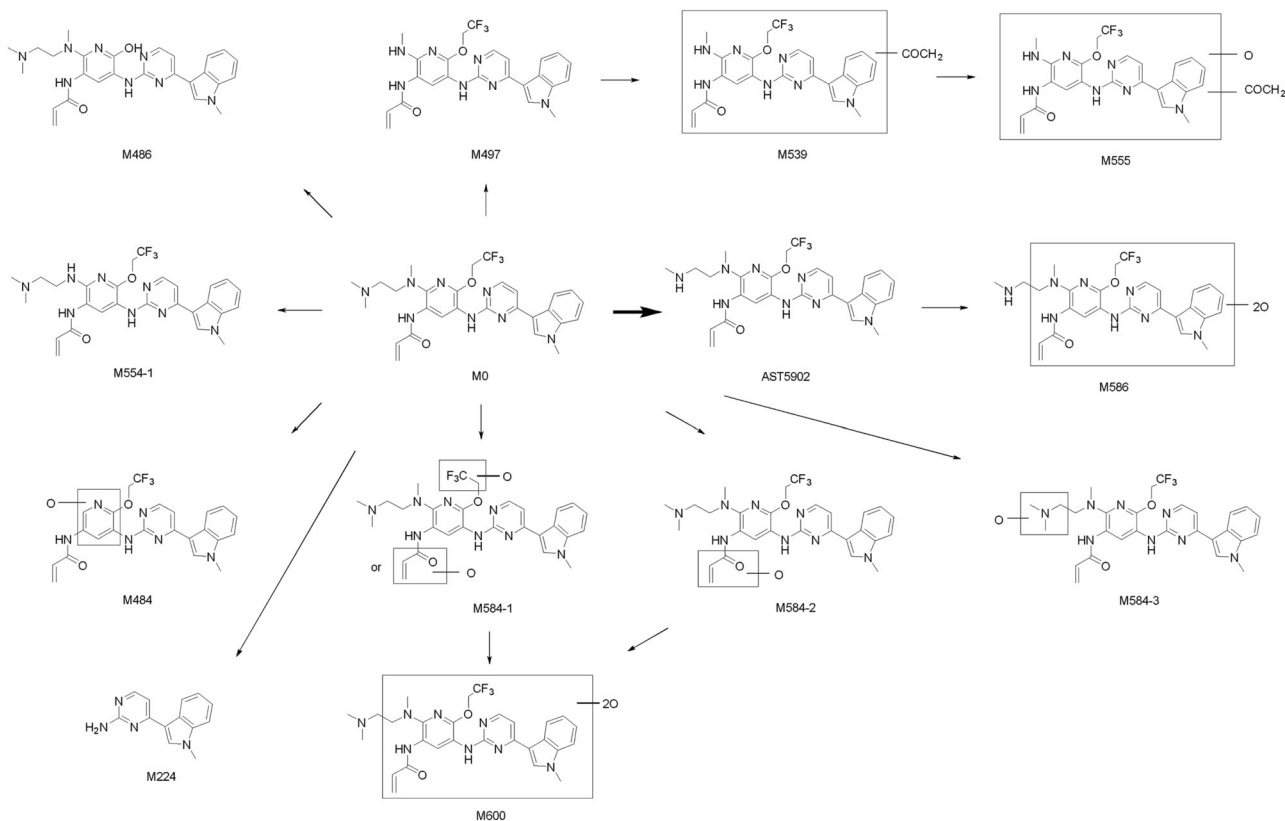


Fig. 5 Proposed metabolic pathway of alflutinib in HLMs. The structure of 13 metabolites were showed. Except for M224, M486, M497, M554-1 and AST5902, the exact modified positions of other metabolites remained unclear

Table 2. Metabolism of alflutinin by recombinant human P450 isoforms

Name	Retention time (min)	Elemental composition	Relative MS area (%)									
			1A2	2A6	2B6	2C8	2C9	2C19	2D6	2E1	3A4	3A5
M0	9.36	C ₂₈ H ₃₁ F ₃ N ₈ O ₂	93.69	95.15	95.84	95.02	91.04	96.18	96.27	95.02	21.07	66.58
M224	5.74	C ₁₃ H ₁₂ N ₄	—	—	1.50	0.74	3.36	0.73	2.46	1.93	38.81	10.14
M484	10.3	C ₂₃ H ₁₉ F ₃ N ₆ O ₃	—	—	—	—	—	—	—	—	2.38	0.61
M486	6.9	C ₂₆ H ₃₀ N ₈ O ₂	0.47	1.36	0.74	0.47	1.03	1.19	—	0.65	—	0.38
M497	9.94	C ₂₄ H ₂₂ F ₃ N ₇ O ₂	—	—	—	—	—	—	—	—	0.66	—
M554-1	7.78	C ₂₇ H ₂₉ F ₃ N ₈ O ₂	0.35	0.68	0.48	0.35	0.60	0.28	0.22	0.52	0.81	0.57
AST5902	9.09	C ₂₇ H ₂₉ F ₃ N ₈ O ₂	—	—	—	1.35	1.79	0.19	—	0.22	9.80	5.93
M555	8.94	C ₂₆ H ₂₄ F ₃ N ₇ O ₄	—	—	—	—	—	—	—	—	0.74	—
M584-1	8.14	C ₂₈ H ₃₁ F ₃ N ₈ O ₃	4.66	—	—	1.19	0.37	0.72	—	—	0.50	3.75
M584-2	8.59	C ₂₈ H ₃₁ F ₃ N ₈ O ₃	—	—	—	—	—	—	—	—	1.26	2.44
M584-3	9.19	C ₂₈ H ₃₁ F ₃ N ₈ O ₃	0.66	2.81	1.45	0.55	1.81	0.72	0.78	1.45	3.56	2.08
M586	6.92	C ₂₇ H ₂₉ F ₃ N ₈ O ₄	—	—	—	—	—	—	—	—	6.25	0.98
M600	7.11	C ₂₈ H ₃₁ F ₃ N ₈ O ₄	0.17	—	—	—	—	—	0.27	0.22	14.14	6.55

Table 3. Effects of the selective inhibitors on the formation of metabolites during HLMs incubations

Name	MS area	Relative MS area (%)									
		HLM									
		ANF	QUE	SPZ	TCL	QD	KET	CMT	ABT	CYP ₃	
Control	1A2	2C8	2C9	2B6/ 2C19	2D6	3A	2E1	CYP ₃			
M0	2.47 × 10 ⁵	89	92	58	61	94	227	87	165		
M224	2.32 × 10 ³	127	70	88	94	80	36	100		26	
M484	2.42 × 10 ³	101	62	89	84	39	—	136		—	
M486	5.77 × 10 ³	147	31	92	86	113	18	131		19	
M497	1.49 × 10 ³	81	37	62	62	40	—	89		—	
M539	1.82 × 10 ³	67	57	62	55	58	—	81		—	
M554-1	2.12 × 10 ³	96	53	58	58	100	109	83		76	
AST5902	7.84 × 10 ⁴	97	32	55	62	54	14	88		2	
M555	2.24 × 10 ³	74	51	65	44	64	0	73		—	
M584-1	1.04 × 10 ³	112	38	65	143	121	59	115		—	
M584-2	1.83 × 10 ³	126	76	85	77	161	—	96		31	
M584-3	1.74 × 10 ³	80	82	99	75	66	32	122		32	
M586	9.00 × 10 ²	117	64	91	111	88	—	111		—	
M600	2.60 × 10 ³	95	85	85	104	93	13	102		12	

in vitro by using the equilibrium dialysis method. The unbound fraction of alflutinin in human plasma ($f_{u,p}$) was estimated to be 7.484% by ADMET Predictor9.5 (Simulation Plus). The values of R_3 for DJJ, QBU and HVN were calculated to be 0.31, 0.26 and 0.28, respectively. All these values were below the cutoff value of 0.8, indicating that the induction potential of alflutinin should be further investigated by mechanistic models or clinical DDI assessment using sensitive index substrates:

$$R_3 = 1/[1 + (d \times E_{max} \times 10 \times I_{max,u}) / (EC_{50} + (10 \times I_{max,u}))]. \quad (1)$$

Enzyme induction of AST5902 on the human CYP3A4 enzyme Considering that the steady-state plasma exposure of AST5902 is comparable to that of alflutinin at a high dose, we evaluated the potential induction of CYP3A4 by AST5902. The results are shown

in Table 5 and Supplementary Fig. S12. At lower concentrations (0.003–0.03 μM), AST5902 could inhibit the mRNA transcription of CYP3A4. With increasing concentration, AST5902 exhibited an induction effect. The maximum induction values for DJJ, QBU and HVN were 1.79-, 4.71- and 3.42-fold, respectively.

After treating DJJ with AST5902 at 3 and 5 μM for 72 h, a significant cell morphological change was observed under the microscope, and cell survival decreased compared to the vehicle group. A similar phenomenon was observed when QBU and HVN were treated with AST5902 at 5 μM for 72 h. For the EC₅₀ values, the two highest concentrations were excluded for DJJ, while only the highest concentration was excluded for QUE and HVN. Similar to alflutinin, the dose–response curve of AST5902 in HVN did not exhibit a sigmoidal curve. Thus, the EC₅₀ of AST5902 in HVN was the concentration of AST5902 at 50% E_{max} (Fig. 7). The C_{max} of AST5902 (80 mg) was 72.5 nM at steady state [22], and the $f_{u,p}$ of AST5902 was estimated to be 7.482% by ADMET Predictor. The values of R_3 for DJJ, QBU, and HVN were 0.78, 0.42, and 0.80, respectively. These results indicate that AST5902 is also likely to cause DDIs when coadministered with a CYP3A4 substrate.

Enzyme induction of rifampin on the human CYP3A4 enzyme Rifampin is a potent CYP3A4 inducer, which remains one of the best choices for clinical DDI studies of CYP3A4 induction. The EC₅₀ of rifampin for CYP3A4 induction in human hepatocytes ranged from 0.1 to 0.33 μM [26–28]. The in vivo concentrations of rifampin were 10–18 μM, and the $f_{u,p}$ of rifampin was 0.175 [27, 29]. To calculate the R_3 value of rifampin, we set the EC₅₀ and unbound plasma concentration to 0.25 μM and 2.5 μM, respectively. It was found that the R_3 values of rifampin were 0.12, 0.05 and 0.10 in DJJ, QBU and HVN, respectively, which are consistent with the findings of clinical trials.

DISCUSSION

Our study revealed that alflutinin was predominantly metabolized by CYP3A4 (78%), and CYP3A4 (79%) was the major enzyme that catalyzes alflutinin to form AST5902. As a substrate of CYP3A4, it is important to assess the effects of CYP3A4 inhibitors or inducers on alflutinin metabolism and pharmacokinetics. Osimertinib, an alflutinin analog, is primarily metabolized by CYP3A4 [30]. Rifampin (a potent CYP3A4 inducer) exerts a moderate effect (2- to 5-fold) on the clinical pharmacokinetics of osimertinib, while itraconazole (a potent CYP3A4 inhibitor) has no remarkable clinical

Table 4. Inhibition of CYP activities in HLMs

CYP isozymes	Probe drug alone	Percentage of residual metabolic activity (%)							
		Alflutinib concentration (μM)							
		0	0.1	0.33	1	3.33	10	33.3	100
CYP1A2	Phenacetin <i>O</i> -deethylation	100	70.4	74.1	91.2	75.3	73.3	78.3	67.2
CYP2B6	Bupropion hydroxylation	100	97.8	97.5	95.2	102	101	95.8	88.8
CYP2C8	Paclitaxel 6 α -hydroxylation	100	103	105	101	102	95.3	82	84.3
CYP2C9	Tolbutamide 4'-hydroxylation	100	94.5	105	108	104	100	99.9	77.1
CYP2C19	(<i>S</i>)-Mephenytoin 4'-hydroxylation	100	94.6	108	109	110	104	93.1	61.3
CYP2D6	Dextromethorphan <i>O</i> -demethylation	100	100	96.4	102	105	112	107	107
CYP3A4	Midazolam 1'-hydroxylation	100	79.6	77.6	77.7	78.4	78	66	62.5
CYP3A4	Testosterone 6 β -hydroxylation	100	100	102	101	112	91.3	82.8	57.9

Table 5. Induction of CYP3A4 mRNA expression in human hepatocytes

Test compound	Concentration (μM)	Maximum fold induction			EC_{50} (μM)			R_3		
		DJJ	QBU	HVN	DJJ	QBU	HVN	DJJ	QBU	HVN
		Alflutinib	0.003–5	9.24	11.2	10.4	0.25	0.24	0.25	0.31
AST5902	0.003–5	1.79	4.71	3.42	0.29	0.13	0.68	0.78	0.42	0.80
Rifampin	10	7.22	19.4	9.46		0.1–0.33		0.12	0.05	0.10

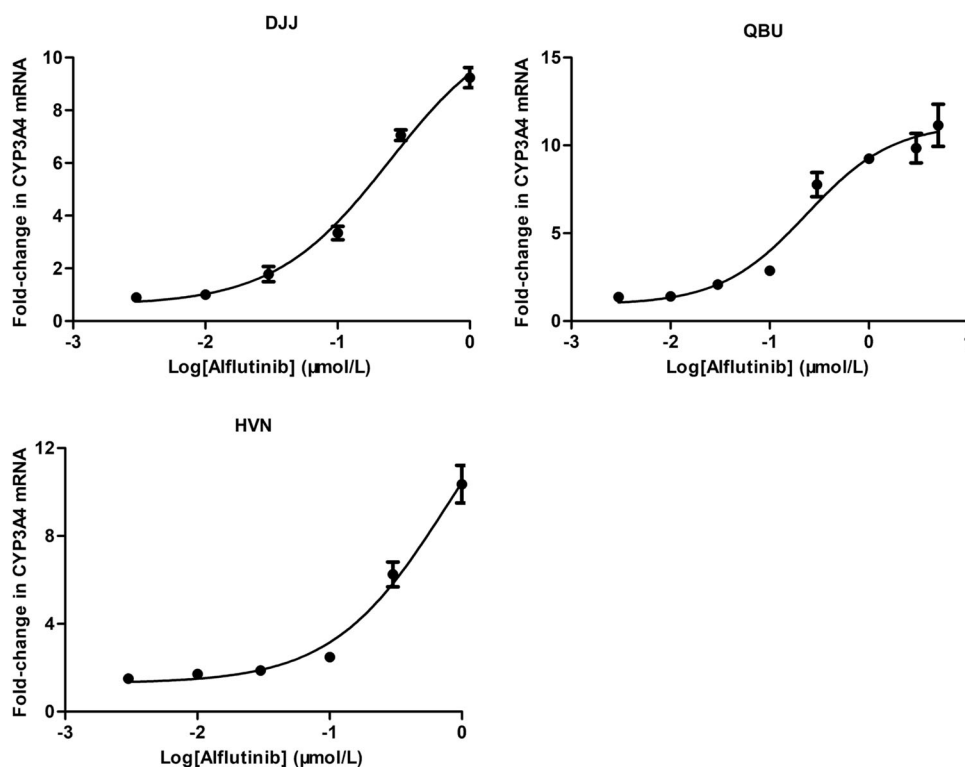


Fig. 6 Dose–response curves for the mRNA expression levels of CYP3A4 induced by alflutinib in DJJ, QBU and HVN. Data are presented as arithmetic mean \pm standard deviation ($n = 3$)

effect on the metabolism of osimertinib (< 1.25 -fold) [31]. The findings of the current phenotyping experiments confirm that alflutinib is a substrate of CYP3A4. In view of the structural similarity between alflutinib and osimertinib, it is most likely that

alflutinib may undergo DDIs when coadministered with CYP3A4 inducers. However, additional investigation is needed to explore the clinical DDIs of alflutinib with CYP3A inducers and inhibitors. The results of this study demonstrated that alflutinib did not

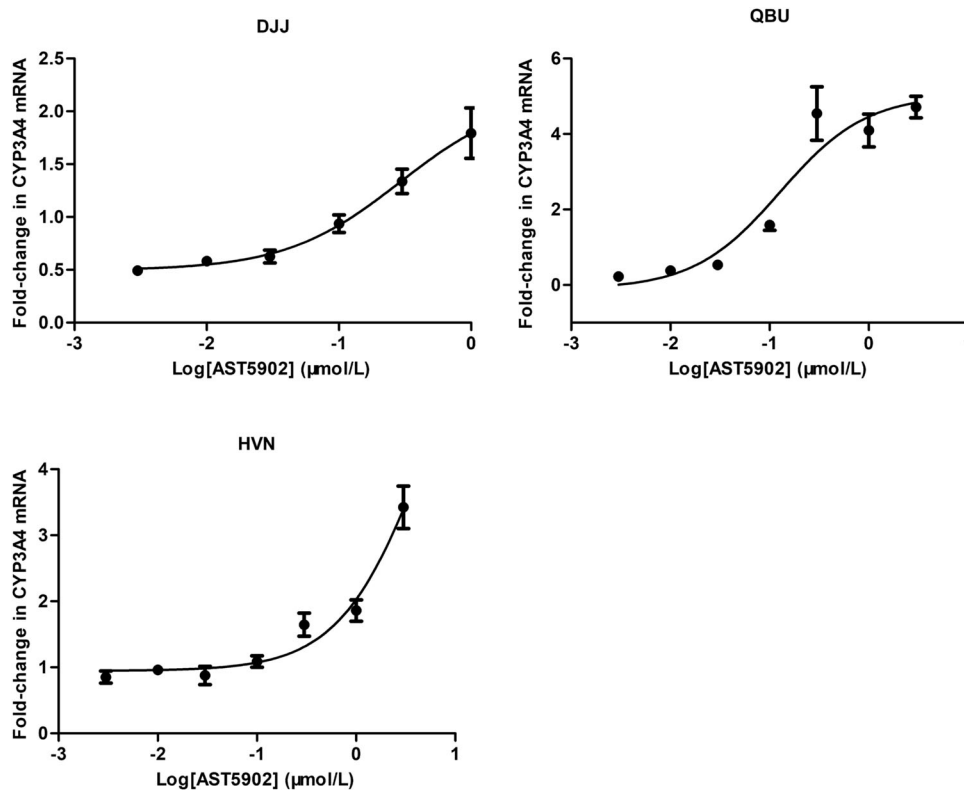


Fig. 7 Dose–response curves for the mRNA expression levels of CYP3A4 induced by AST5902 in DJJ, QBU and HVN. Data are presented as arithmetic mean \pm standard deviation ($n = 3$)

inhibit P450 in vitro; however, it could be a potent CYP3A4 inducer. We also investigated the potential of alflutinib to act as an inducer of CYP1A2 and CYP2B6, and the study endpoint was enzyme activity levels using a probe substrate. Alflutinib produced a change in CYP1A2 and CYP2B6 enzyme activity that was less than the cutoff value of 40% of the positive control (Supplementary Table S3 and S4). Thus, alflutinib did not induce CYP1A2 and CYP2B6 in vitro. We did not investigate whether alflutinib is a CYP2C inducer, which is a limitation of our study.

Alflutinib is the first new drug that exhibits strong CYP3A4 enzyme induction and will undergo a clinical DDI study in China. Induction of drug-metabolizing enzymes is not as common as inhibition, and CYP3A4 induction is not generally considered a concern for safety. However, CYP3A4 induction can lead to subtherapeutic drugs and/or increase the formation of active or reactive metabolites [26]. In human hepatocytes, 1 μ M alflutinib could exhibit a higher E_{\max} value for CYP3A4 induction compared to 10 μ M rifampin in DJJ and HVN. Rifampin has been recognized as a potent CYP3A inducer, but alflutinib exhibited similar or even greater E_{\max} . This indicates that alflutinib can serve as a novel CYP3A inducer. The maximum concentration of alflutinib was set to 5 μ M, which exhibited toxic effects on DJJ and HVN but might be insufficient for QBU to achieve E_{\max} . Alflutinib exerts strong induction potential for CYP3A4, and the C_{\max} of alflutinib at therapeutic doses is likely to induce CYP3A4 in vivo. However, alflutinib is less likely to have a profound effect on the CYP3A4 substrate, similar to rifampin, because of its dosage. Therefore, it is necessary to conduct a clinical trial to assess the CYP3A4 induction potential of alflutinib. Considering the high exposure of AST5902 and the structures of alflutinib and AST5902, we also evaluated the CYP3A4 induction potential of AST5902. At low concentrations, AST5902 inhibited the mRNA transcription of CYP3A4, but the underlying mechanisms remain unclear.

Compared to alflutinib and rifampin, the in vitro induction effects of AST5902 were found to be less significant. However, given the plasma exposure of AST5902, AST5902 is also likely to cause a clinical DDI with CYP3A4-sensitive substrates.

Upon incubation of 3 μ M alflutinib with human hepatocytes at 37 $^{\circ}$ C for 3 h, the primary metabolite was identified as AST5902, accounting for 52% of the remaining alflutinib concentration. Other metabolites accounted for less than 1.2% of alflutinib (unpublished data). In addition, AST5902 exerted CYP3A4 induction potential, which might contribute to the induction effect of alflutinib.

In phase I/II clinical trials, the C_{\max} and AUC of a single-dose alflutinib were elevated in a dose-dependent manner among NSCLC patients in the dose range of 20–240 mg [23]. After multiple doses, the increase in alflutinib exposure was less than that of a single dose. The AUC of AST5902 greatly increased, even exceeding that of alflutinib in the 240 mg dosage group. In addition, alflutinib showed a time-dependent and dose-dependent increase in clearance (CL/F) following multiple doses. CYP phenotyping studies and CYP enzyme induction indicated that alflutinib was a substrate and inducer of CYP3A4. Thus, the self-induction of alflutinib may be the reason for the phenomenon observed in clinical trials. Given the exposure of human alflutinib at an 80 mg dose, alflutinib is speculated to activate clinical pharmacokinetic DDIs when coadministered with CYP3A4-sensitive substrates, including midazolam and triazolam. Considering that the activation of pregnane X receptor (PXR) can induce CYP3A and CYP2C, further evaluation of the potential of alflutinib to induce CYP2C should be conducted [32].

In conclusion, alflutinib is a substrate and potent inducer of CYP3A4 but not an inhibitor of CYP450 enzymes. Thus, clinically relevant pharmacokinetic DDIs are likely to take place when

alflutinin serves as a victim coadministered with CYP inducers or inhibitors or acts as a perpetrator coadministered with CYP3A4-sensitive substrates. Alflutinin is the first drug developed in China that exhibits potent CYP3A4 induction, and related clinical trials will be conducted in the future. Nevertheless, it is necessary to evaluate the effects of self-induction on the efficacy of alflutinin.

ACKNOWLEDGEMENTS

This work was supported by the Strategic Priority Research Program of the Chinese Academy of Sciences [XDA12050306] and the National Natural Science Foundation of China [81521005, 81903701].

AUTHOR CONTRIBUTIONS

XYL, DFZ, YJ, and QYZ participated in the research design; XYL, ZTG, ZDC, and JLZ conducted the experiments; XYL and YFZ performed data analysis; XYL, DFZ, and XXD wrote or contributed to the writing of the manuscript.

ADDITIONAL INFORMATION

The online version of this article (<https://doi.org/10.1038/s41401-020-0389-3>) contains supplementary material, which is available to authorized users.

Competing interests: The authors declare no competing interests.

REFERENCES

1. Bray F, Ferlay J, Soerjomataram I, Siegel RL, Torre LA, Jemal A. Global cancer statistics 2018: globocan estimates of incidence and mortality worldwide for 36 cancers in 185 countries. *CA Cancer J Clin.* 2018;68:394–424.
2. Feng RM, Zong YN, Cao SM, Xu RH. Current cancer situation in China: good or bad news from the 2018 global cancer statistics? *Cancer Commun.* 2019;39:22.
3. Sun S, Schiller JH, Spinola M, Minna JD. New molecularly targeted therapies for lung cancer. *J Clin Invest.* 2007;117:2740–50.
4. Alvarez M, Roman E, Santos ES. New targets for non-small-cell lung cancer therapy. *Expert Rev Anticanc.* 2007;7:1423–37.
5. Molina JR, Yang P, Cassivi SD, Schild SE, Adjei AA. Non-small cell lung cancer: epidemiology, risk factors, treatment, and survivorship. *Mayo Clin Proc.* 2008;83:584–94.
6. Herbst RS, Morgensztern D, Boshoff C. The biology and management of non-small cell lung cancer. *Nature.* 2018;553:446–54.
7. Yarden Y, Sliwkowski MX. Untangling the ErbB signalling network. *Nat Rev Mol Cell Biol.* 2001;2:127–37.
8. Lynch TJ, Bell DW, Sordella R, Gurubhagavatula S, Okimoto RA, Brannigan BW, et al. Activating mutations in the epidermal growth factor receptor underlying responsiveness of non-small-cell lung cancer to gefitinib. *N Engl J Med.* 2004;350:2129–39.
9. Sharma SV, Bell DW, Settleman J, Haber DA. Epidermal growth factor receptor mutations in lung cancer. *Nat Rev Cancer.* 2007;7:169–81.
10. Fukuoka M, Wu YL, Thongprasert S, Sunpaweravong P, Leong SS, Sriuranpong V, et al. Biomarker analyses and final overall survival results from a phase III, randomized, open-label, first-line study of gefitinib versus carboplatin/paclitaxel in clinically selected patients with advanced non-small-cell lung cancer in Asia (IPASS). *J Clin Oncol.* 2011;29:2866–74.
11. Zhou C, Wu YL, Chen G, Feng J, Liu XQ, Wang C, et al. Erlotinib versus chemotherapy as first-line treatment for patients with advanced EGFR mutation-positive non-small-cell lung cancer (OPTIMAL, CTONG-0802): a multicentre, open-label, randomised, phase 3 study. *Lancet Oncol.* 2011;12:735–42.

12. Paz-Ares L, Tan EH, O'Byrne K, Zhang L, Hirsh V, Boyer M, et al. Afatinib versus gefitinib in patients with EGFR mutation-positive advanced non-small-cell lung cancer: overall survival data from the phase IIb LUX-Lung 7 trial. *Ann Oncol.* 2017;28:270–7.
13. Kim Y, Lee SH, Ahn JS, Ahn MJ, Park K, Sun JM. Efficacy and safety of afatinib for EGFR-mutant non-small cell lung cancer, compared with gefitinib or erlotinib. *Cancer Res Treat.* 2019;51:502–9.
14. Wu YL, Cheng Y, Zhou X, Lee KH, Nakagawa K, Niho S, et al. Dacomitinib versus gefitinib as first-line treatment for patients with EGFR-mutation-positive non-small-cell lung cancer (ARCHER 1050): a randomised, open-label, phase 3 trial. *Lancet Oncol.* 2017;18:1454–66.
15. Ramalingam SS, O'Byrne K, Boyer M, Mok T, Janne PA, Zhang H, et al. Dacomitinib versus erlotinib in patients with EGFR-mutated advanced nonsmall-cell lung cancer (NSCLC): pooled subset analyses from two randomized trials. *Ann Oncol.* 2016;27:423–9.
16. Pao W, Miller VA, Politi KA, Riely GJ, Somwar R, Zakowski MF, et al. Acquired resistance of lung adenocarcinomas to gefitinib or erlotinib is associated with a second mutation in the EGFR kinase domain. *Plos Med.* 2005;2:225–35.
17. Han W, Du Y. Recent development of the second and third generation irreversible epidermal growth factor receptor inhibitors. *Chem Biodivers.* 2017;14:e1600372.
18. Cheng H, Nair SK, Murray BW. Recent progress on third generation covalent EGFR inhibitors. *Bioorg Med Chem Lett.* 2016;26:1861–8.
19. Mok TS, Wu YL, Ahn MJ, Garassino MC, Kim HR, Ramalingam SS, et al. Osimertinib or platinum-pemetrexed in EGFR T790M-positive lung cancer. *N Engl J Med.* 2017;376:629–40.
20. Soria JC, Ohe Y, Vansteenkiste J, Reungwetwattana T, Chewaskulyong B, Lee KH, et al. Osimertinib in untreated EGFR-mutated advanced non-small-cell lung cancer. *N Engl J Med.* 2018;378:113–25.
21. Kim ES. Olmutinib: first global approval. *Drugs.* 2016;76:1153–7.
22. Shi YK, Zhang SC, Hu XS, Feng JF, Ma ZY, Zhou JY, et al. Safety, clinical activity and pharmacokinetics of alflutinin (AST2818) in advanced NSCLC patients with EGFR T790M mutation. *J Thorac Oncol.* 2020; in press.
23. Liu XY, Li W, Zhang YF, Jiang Y, Zhao QY, Zhong DF. Simultaneous determination of alflutinin and its active metabolite in human plasma using liquid chromatography–tandem mass spectrometry. *J Pharm Biomed Anal.* 2019;176:112735.
24. Rodrigues AD. Integrated cytochrome P450 reaction phenotyping. *Biochem Pharmacol.* 1999;57:465–80.
25. Fahmi OA, Ripp SL. Evaluation of models for predicting drug–drug interactions due to induction. *Expert Opin Drug Met.* 2010;6:1399–416.
26. Xu Y, Zhou Y, Hayashi M, Shou M, Skiles GL. Simulation of clinical drug–drug interactions from hepatocyte CYP3A4 induction data and its potential utility in trial designs. *Drug Metab Dispos.* 2011;39:1139–48.
27. Shou M, Hayashi M, Pan Y, Xu Y, Morrissey K, Xu L, et al. Modeling, prediction, and in vitro in vivo correlation of CYP3A4 induction. *Drug Metab Dispos.* 2008;36:2355–70.
28. Dixit V, Moore A, Tsao H, Hariprasad N. Application of micropatterned cocultured hepatocytes to evaluate the inductive potential and degradation rate of major xenobiotic metabolizing enzymes. *Drug Metab Dispos.* 2016;44:250–61.
29. Garg V, Chandorkar G, Yang Y, Adda N, McNair L, Alves K, et al. The effect of CYP3A inhibitors and inducers on the pharmacokinetics of telaprevir in healthy volunteers. *Br J Clin Pharmacol.* 2013;75:431–9.
30. Dickinson PA, Cantarini MV, Collier J, Frewer P, Martin S, Pickup K, et al. Metabolic disposition of osimertinib in rats, dogs, and humans: insights into a drug designed to bind covalently to a cysteine residue of epidermal growth factor receptor. *Drug Metab Dispos.* 2016;44:1201–12.
31. Vishwanathan K, Dickinson PA, So K, Thomas K, Chen YM, De Castro Carpeno J, et al. The effect of itraconazole and rifampicin on the pharmacokinetics of osimertinib. *Br J Clin Pharmacol.* 2018;84:1156–69.
32. Tolson AH, Wang H. Regulation of drug-metabolizing enzymes by xenobiotic receptors: PXR and CAR. *Adv Drug Deliv Rev.* 2010;62:1238–49.